Transition from slow and frozen to superluminal and backward light through loss or gain in dispersion-engineered waveguides

Thomas P. White[1,2,*] and Andrey A. Sukhorukov[1]

[1]*Nonlinear Physics Centre and Centre for Ultrahigh-Bandwidth Devices for Optical Systems (CUDOS), Research School of Physics and Engineering, Australian National University, Canberra, Australian Capital Territory 0200, Australia*

[2]*Laser Physics Centre, Research School of Physics and Engineering, Australian National University, Canberra, Australian Capital Territory 0200, Australia*

(Received 8 October 2011; published 11 April 2012)

We describe the generic effects of loss or gain on pulse propagation in photonic-crystal and plasmonic waveguides that support "frozen" or "in-band" slow light at dispersion inflection points in the absence of loss (or gain). Using an analytical perturbation theory, we find that propagating and evanescent modes hybridize when loss exceeds a certain threshold, resulting in a reduced attenuation rate and switching from slow to superluminal velocity. Numerical simulations for photonic-crystal waveguides reveal the dynamic nature of this transition with forward-backward pulse velocity oscillations for loss above the threshold. Importantly, we show that the light intensity is enhanced close to the input end of the waveguide even under strong material losses, indicating the potential for slow-light enhancement of optical effects, even in such lossy waveguides.

DOI: 10.1103/PhysRevA.85.043819 PACS number(s): 42.25.Bs, 42.79.Gn, 42.70.Qs

I. INTRODUCTION

Enhancement of light-matter interactions in slow-light (SL) waveguides offers new opportunities for tunable delays, switching, and monitoring of optical pulses in compact photonic structures [1]. SL occurs naturally for optical frequencies at the edges of photonic transmission bands, however, in this regime the dispersion relation is typically quadratic, leading to strong group-velocity dispersion and undesirable pulse broadening [2]. Moreover, there are significant challenges to coupling light efficiently into band-edge SL modes. For these reasons, there is much interest in dispersion-engineered waveguides which support SL inside an optical transmission band, as has been proposed [3] and experimentally demonstrated [4–7] for photonic-crystal waveguides and suggested for plasmonic guiding structures [8,9]. Waveguides featuring a dispersion inflection point can support SL modes with zero group-velocity dispersion (GVD), while at the same time providing very efficient coupling of input and output light without the need for complicated transitions [10], even in the "frozen light" regime at zero group velocity [11,12].

A fundamentally interesting and practically important problem is the effect of material loss or gain on optical pulse propagation in the regime of SL. Intrinsic losses may arise from material properties such as absorption in metallic plasmonic waveguides or gases in hollow fibers. Alternatively, loss or gain can be introduced through pumping in active media or through nonlinear wave mixing based on Raman processes [1]. On the one hand, SL can enhance the effects of loss or gain [13,14]. On the other hand, the presence of loss or gain can dramatically change the waveguide dispersion [15–17], in particular leading to the appearance of superluminal dispersion points with infinite group velocity close to the SL frequency region. For SL associated with photonic band edges, the presence of loss limits the maximum achievable slowdown factor [18–20]. It was suggested that the SL regime can be restored by the introduction of active amplifying layers in metal-dielectric waveguides [21–23], and tunable slow-light manipulation was demonstrated in amplifying semiconductor ring resonators [24].

Here, we reveal through analytical analysis and numerical simulations, the generic effects of material loss or gain on wave propagation in dispersion-engineered SL waveguides, and identify unique features distinct from band-edge SL considered previously [18–20]. We predict a dynamic transition from slow- to superluminal propagation at a threshold loss magnitude, manifesting as pulse oscillations forward and backward in time due to hybridization and the interference of propagating and evanescent waves. Most importantly, the mode interference results in pulse intensity enhancement close to the waveguide boundary even under strong losses, indicating a potential for the practical realization of the predicted effects. These results have direct implications for engineered slow light in plasmonic waveguides [8,9] while also highlighting important considerations for fundamental studies of frozen light phenomena in periodic media [11]. We note that scattering losses can also affect light propagation [13], yet there have been strong advances in structure engineering for their minimization [25] and we neglect them from our consideration.

The paper is organized as follows. In Sec. II we formulate a perturbation theory for dispersion-engineered slow-light waveguides. We apply this theory in Sec. III to describe analytically the generic effects of loss (or gain) on waveguide dispersion and predict its critical transition at a threshold loss magnitude. In Sec. IV, we confirm the analytical results with direct numerical simulations for lossy photonic-crystal waveguides, and additionally demonstrate intensity enhancement even under strong losses. Then, in Sec. V we analyze pulse dynamics in these waveguides and reveal temporal oscillations between forward and backward propagation associated with

*thomas.white@anu.edu.au; Current address: Centre for Sustainable Energy Systems, Research School of Engineering, Australian National University, ACT 0200, Australia.

the slow- to fast-velocity transition. We summarize our findings and provide an outlook in Sec. VI.

II. PERTURBATION THEORY FOR DISPERSION-ENGINEERED SLOW-LIGHT WAVEGUIDES

As a starting point, we consider an SL waveguide in which the dispersion $\omega(k)$ is engineered to suppress GVD [i.e., $\alpha = \partial^2\omega/\partial k^2 = 0$ at a frequency $\omega_0 = \omega(k_0)$, where k is the wave number]. Then, a Taylor expansion of the dispersion curve to third order can be written as

$$\omega(k) \simeq \omega_0 + v_{g,0}(k - k_0) + \beta(k - k_0)^3, \tag{1}$$

where $v_{g,0} = \partial\omega/\partial k|_{k_0}$ is the group velocity and $\beta = (1/6)(\partial^3\omega/\partial k^3)|_{k_0}$. The absence of the second-order term is due to GVD suppression, associated with an inflection point in the dispersion dependence.

While the analysis presented here is generic to any inflection-point slow-light waveguide, for the numerical examples throughout this paper we consider a specially designed photonic-crystal (PhC) waveguide shown in Fig. 1(a). The slow-light section, (ii), consists of a two-dimensional PhC slab with refractive index $n = 2.83$, period a, and holes of radius $r = 0.3a$. A missing line of holes forms the waveguide core, and the first two rows of holes on either side are shifted parallel to the waveguide axis by $0.3a$ and $0.425a$, respectively.

The fundamental TE-polarized (electric field in the plane of the PhC) mode dispersion has an inflection point [see solid curve in Fig. 1(b)] where the group index (slowdown factor) is $n_g \approx 280$ in a narrow wavelength range [see Fig. 1(d)]. The dispersion is well approximated by Eq. (1) with $k_0 a/(2\pi) = 0.6131$, $\omega_0 a/(2\pi c) = 0.264585$, $v_{g,0} = c/280$, and $\beta = 16c(2\pi/a)^2$.

To study the influence of material loss (or gain) on the waveguide dispersion, we consider the effect of a small imaginary part of the refractive index $n = n_r + in_i$. The corresponding complex permittivity is given by $\epsilon \simeq \epsilon_r + i\epsilon_i$, where ϵ_r is that of the lossless waveguide and $\epsilon_i = 2n_r n_i$. From first-order perturbation theory [19], the small change in ϵ produces a small frequency shift

$$\Delta\omega = -i\frac{1}{2}\omega f\frac{\epsilon_i}{\epsilon_r}. \tag{2}$$

Here $f = \langle E|\epsilon_i|E\rangle_V/\langle E|\epsilon_r|E\rangle$ describes the proportion of the total mode energy in the volume V comprising the lossy dielectric, where E is the electric field mode profile.

Then we replace ω_0 in Eq. (1) with $\omega_0 + \Delta\omega_0$, where $\Delta\omega_0$ is given by Eq. (2) evaluated at ω_0, and invert the resulting equation to solve for $k(\omega)$ at real ω. The function $\omega(k)$ is cubic and hence there are three solutions at each frequency. When there is no loss ($n_i = 0$), we obtain one real k_1 and a pair of complex solutions, $k_2 = k_3^*$, which correspond to evanescent modes. The dispersion of the evanescent mode which decays in the propagation direction [$\mathrm{Im}(k) \geqslant 0$] is plotted as dashed curves in Figs. 1(b) and 1(c). We note that the simultaneous presence of propagating and evanescent modes is a characteristic feature of a dispersion inflection point, and this was recently demonstrated experimentally for dispersion-engineered photonic-crystal waveguides [26,27].

III. EFFECT OF LOSS ON WAVEGUIDE DISPERSION

We now analyze the effect of loss on the waveguide dispersion. All three solutions $k(\omega)$ are complex for $n_i > 0$, but only two have $\mathrm{Im}(k) > 0$ corresponding to a physically relevant situation of wave decay in the propagation direction. We show dispersion curves for the two modes for a set of increasing n_i in Fig. 2. When $n_i = 2 \times 10^{-4}$, the dispersion of $\mathrm{Re}(k)$ in Fig. 2(a) closely resembles the lossless case in Fig. 1(b), apart from a slight distortion close to the inflection point. Accordingly, the zero GVD condition is also preserved. On the other hand, what was previously the propagating mode

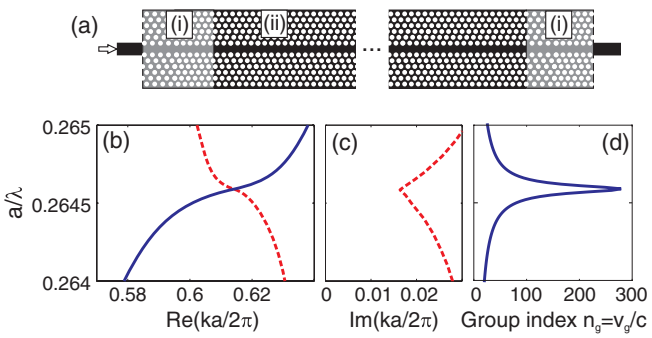

FIG. 1. (Color online) (a) PhC waveguide geometry. (b) Re(k) dispersion curves for the propagating mode (solid line) and first evanescent mode (dashed line) in the slow-light waveguide. (c) Corresponding Im(k) curve for the evanescent mode. (d) Group index of the propagating mode, where the slow-light region is associated with the dispersion inflection point.

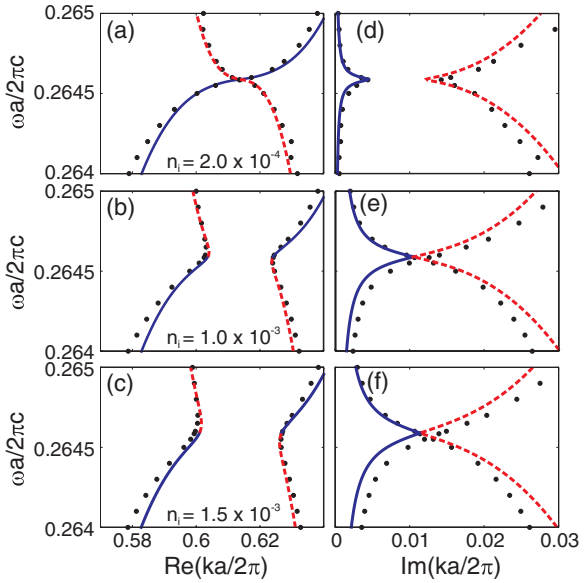

FIG. 2. (Color online) (a–c) Real and (d–f) imaginary wavevector components of the waveguide modes for different values of loss. The solid and dashed curves are calculated using the perturbation model and dots are numerical FDTD results. The line type follows the mode classification in the absence of losses as either propagating (solid line) or evanescent (dashed line).

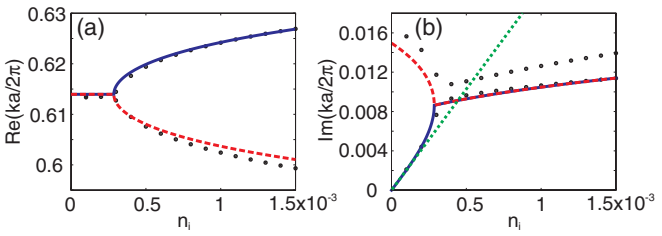

FIG. 3. (Color online) (a) Real and (b) imaginary wave-vector components of the waveguide modes at the inflection point frequency plotted as a function of n_i. The solid and dashed curves are calculated using the perturbation model and dots are numerical FDTD results. Straight dotted green line in (b) shows the asymptotic dependence for low loss according to Eq. (4).

with purely real k now has a small $\mathrm{Im}(k)$ component that peaks at the inflection point frequency due to slow-light enhancement of the loss, see Fig. 2(d).

As n_i increases, the propagating and evanescent modes form hybrid states close to the inflection point as shown in Figs. 2(b) and 2(e) and Figs. 2(c) and 2(f). This coupling manifests as an avoided crossing of the $\mathrm{Re}(k)$ dispersion curves and a corresponding crossing of the $\mathrm{Im}(k)$ curves such that the decay rate of both modes is equal at ω_0. Note also that the inflection feature of the original dispersion curve in Fig. 1(b) has disappeared, dramatically changing the dispersion: Instead of slow light, the group velocity becomes superluminal as the dispersion dependence acquires a vertical slope in the vicinity of ω_0. Such dispersion features are not unique to the system considered here, and superluminal group velocity has been associated with evanescent modes in a number of other contexts [28,29]. These states do not violate causality because purely evanescent modes are nonpropagating.

From the analytic form of the cubic solutions of $k(\omega)$ we find that the loss threshold for the mode hybridization is

$$\epsilon_i^{\mathrm{th}} = \left(\frac{3}{\beta}\right)^{1/2} \frac{4\epsilon_r v_{g,0}^{3/2}}{9\omega_0}, \tag{3}$$

which corresponds to $\epsilon_i^{\mathrm{th}} = 1.2 \times 10^{-3}$ or $n_i^{\mathrm{th}} = 2.2 \times 10^{-4}$ for the SL PhC waveguide shown in Fig. 1(a).

The mode hybridization is evident in the dependencies of mode dispersion at the inflection point frequency (ω_0) shown in Fig. 3. When the loss is below the threshold value, both modes have equal $\mathrm{Re}(k)$, as for the lossless case, while the values of $\mathrm{Im}(k)$ approach each other as $\epsilon_i \to \epsilon_i^{\mathrm{th}}$. Once the loss passes the threshold value, the $\mathrm{Re}(k)$ curves split, while $\mathrm{Im}(k)$ is equal for the two modes.

For small losses below the threshold, $\epsilon_i < \epsilon_i^{\mathrm{th}}$, perturbation theory predicts the enhancement of the propagating mode decay rate proportional to the slowdown factor

$$\mathrm{Im}(k) \simeq \frac{1}{2v_{g,0}} \omega_0 f \frac{\epsilon_i}{\epsilon_r}, \tag{4}$$

and we show this dependence by the dotted (green) line in Fig. 3(b).

Above the threshold, $\epsilon_i > \epsilon_i^{\mathrm{th}}$, the decay rate increases much more gradually with increasing material loss, remaining below

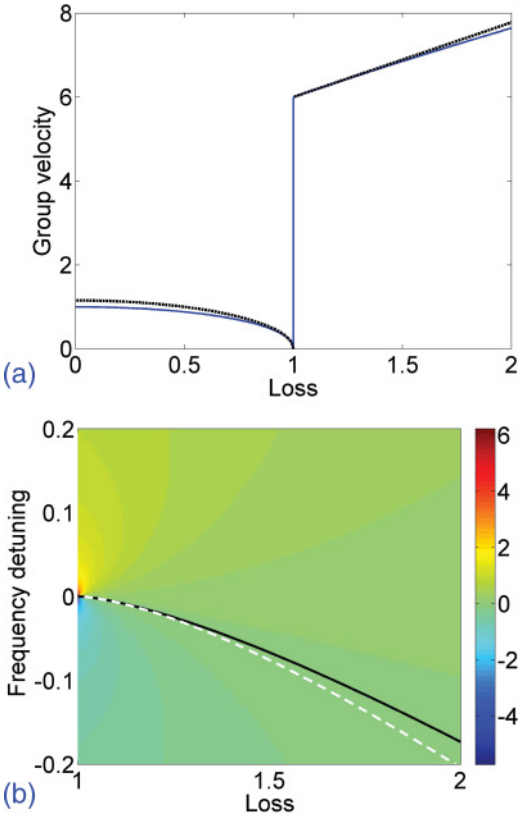

FIG. 4. (Color online) (a) Normalized group velocity ($v_g/v_{g,0}$) for the first mode vs. normalized loss ($\epsilon_i/\epsilon_i^{\mathrm{th}}$) at the frequency ω_0. Solid line: numerical calculation using the perturbation model; dashed lines: asymptotic approximations close to the threshold loss value according to Eqs. (6) and (7). (b) Density plot of inverse group velocity ($v_g^{-1}v_{g,0}$) for the mode with larger $\mathrm{Re}(k)$ vs. normalized loss ($\epsilon_i/\epsilon_i^{\mathrm{th}}$) and frequency detuning [$(\omega-\omega_0)\beta^{1/2}v_{g,0}^{-3/2}$] calculated using the perturbation model. Solid black line: zero contour line corresponding to infinite group velocity; dashed white line: analytical approximation of the contour line according to Eq. (8).

the level of

$$\mathrm{Im}(k) \simeq \left(\frac{v_{g,0}}{3\beta}\right)^{1/2} + \frac{1}{12v_{g,0}} \omega_0 f \frac{\epsilon_i - \epsilon_i^{\mathrm{th}}}{\epsilon_r}. \tag{5}$$

Note that here the multiplier in front of ϵ_i is decreased by a factor of 6 compared to the case of small losses of Eq. (4).

The group velocity also exhibits nontrivial behavior due to mode hybridization. In particular, the group velocity at the central frequency (ω_0) depends nonmonotonically on the loss coefficient, see Fig. 4(a). The plots show results for the first mode; the other mode has identical group velocity, but with the opposite sign. By analyzing the dispersion relation, we determine that below, but close to the hybridization threshold (for $\epsilon_i \to \epsilon_i^{\mathrm{th}}$ while $\epsilon_i < \epsilon_i^{\mathrm{th}}$), the group velocity at the inflection point frequency ω_0 is

$$v_g(\omega_0)\big|_{\epsilon_i<\epsilon_i^{\mathrm{th}}} \simeq \pm v_{g,0} \frac{2}{\sqrt{3}} \sqrt{1-\left(\epsilon_i/\epsilon_i^{\mathrm{th}}\right)^2}, \tag{6}$$

where the sign "+" corresponds to the first mode (with smaller loss) and "−" to the second mode (which has a larger decay rate). Interestingly, as the threshold is approached from below, the group velocity at the inflection point approaches zero,

corresponding to the "frozen light" regime. As the modes hybridize, the group-velocity value changes abruptly and just above the threshold we have

$$v_g(\omega_0)\big|_{\epsilon_i>\epsilon_i^{\rm th}} \simeq \pm 6 v_{g,0}\left[1+(8/27)\left(\epsilon_i/\epsilon_i^{\rm th}-1\right)\right]. \quad (7)$$

We note that the group velocity above the threshold is increased six times compared to the low-loss regime, and it corresponds to a six-fold decrease in decay rate versus material loss as discussed above for Eq. (5). The analytical dependencies of Eqs. (6) and (7) are shown in Fig. 4(a) with dashed lines, which are very close to the exact numerical values plotted with a solid line.

Another important feature of group velocity is the appearance of superluminal and even infinite group-velocity points corresponding to vertical slopes of the dispersion dependencies as seen in Fig. 2(b) and 2(c). The interesting effect here is that the appearance of such dispersion regions can be tuned to different frequencies purely by varying the material loss. We plot the dependence of the inverse velocity for the mode with larger Re(k) on the loss coefficient and frequency detuning in Fig. 4(b). The black line follows the $v_g^{-1}=0$ contour where the group velocity becomes infinite. For the other mode the plot appears the same but flipped to opposite frequency detunings. The frequencies at which the group velocity becomes infinite can be found approximately as

$$\omega_\infty \simeq \omega_0 \pm \frac{2v_{g,0}^{3/2}}{27\beta^{1/2}} \frac{\left[\left(\epsilon_i/\epsilon_i^{\rm th}\right)^2-1\right]^{3/2}}{1+(8/27)\left[\left(\epsilon_i/\epsilon_i^{\rm th}\right)^2-1\right]}. \quad (8)$$

We show this dependence with a dashed white line in Fig. 4(b), which is in good agreement with the numerically calculated black zero-level contour line.

Finally, we note that since our analytical results do not depend on the sign of ϵ_i, we can similarly predict the effects of material gain.

IV. NUMERICAL SIMULATIONS FOR LOSSY PHOTONIC-CRYSTAL WAVEGUIDES

To verify the accuracy of the simple perturbation model, we perform two-dimensional finite-difference time-domain (FDTD) simulations of optical pulse propagation in PhC waveguides with weak material absorption. The geometry for these simulations is shown in Fig. 1(a). Light is launched from a narrow ridge waveguide into a PhC waveguide (i) before entering the slow-light waveguide (ii). Section (i) supports a relatively fast mode with $n_g \approx 5$ at ω_0, and provides efficient coupling to the ridge waveguide and to section (ii) [10,30]. While this is not essential to the analysis, it simplifies the numerical simulations by reducing back reflections and ensuring high transmission into the slow-light waveguide (ii) at all wavelengths. Here, waveguide (i) is formed by increasing the lattice constant of waveguide (ii) by 7% in the direction parallel to the waveguide axis. Light is coupled out in an identical way after propagation through 96 periods of waveguide (ii).

To evaluate the dispersion properties of waveguide (ii) we first calculate the steady-state fields in the waveguide for a range of frequencies near the inflection point and then apply a Bloch-mode extraction technique to determine simultaneously

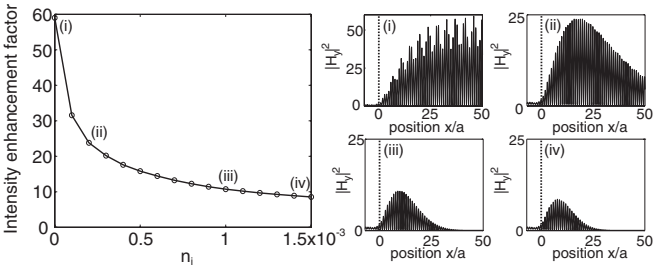

FIG. 5. Left: Field enhancement in the slow-light PhC waveguide as a function of n_i. (i)–(iv): $|H_y|^2$ field on the waveguide axis at points (i)–(iv) marked on the left plot.

both the complex wave-vector components and field profiles of all the waveguide modes [31]. The results of the FDTD dispersion extraction are plotted as dots in Figs. 2 and 3, where the lines correspond to perturbation model results.

Recall that the perturbation model takes as input only the unperturbed dispersion of the propagating mode and the modal overlap with the lossy material (f), Eq. (2). We determine that $f=0.77$ using the mode profile at the inflection point frequency. The agreement with the numerical simulation is remarkable; the simple model reproduces all key features of the mode hybridization, both qualitatively and quantitatively. The only minor deviation is seen in Fig. 3(b) where the imaginary wave-vector components extracted from the FDTD simulations are not exactly equal in the region $\epsilon_i > \epsilon_i^{\rm th}$ whereas they are equal in the analytical model. This difference may be due to a slight frequency shift of the dispersion curves with increasing loss, which is not accounted for when plotting the dispersion at fixed frequency ω_0.

In the absence of losses, the light intensity can increase in the waveguide inversely proportional to the group velocity [10]. The numerical simulations here also allow us to investigate whether lossy slow-light waveguides of this type could still provide the increased intensities required for enhanced nonlinear effects. This is a nontrivial question since, not only does the loss directly reduce the field intensity inside the waveguide, but the reshaping of the dispersion curves changes the group velocity. Figure 5 shows the maximum intensity enhancement at the inflection point as a function of n_i. The enhancement is defined as the ratio of the maximum value of $|H_y|^2$ in the slow-light region to that in the input waveguide, where H_y is the magnetic field component perpendicular to the plane of the PhC. The figures on the right show the field profiles along the waveguide for several values of n_i. The results show that it is possible to achieve an order of magnitude enhancement in the waveguide even in the presence of loss on the scale of $n_i = 10^{-3}$. While such high loss would clearly not allow long propagation distances, it may still be possible to observe enhanced nonlinear effects such as third-harmonic generation, which has been measured in the first few microns of silicon slow-light PhC waveguides [32].

V. SLOW AND BACKWARD PULSE DYNAMICS

We now study the propagation dynamics of light pulses in dispersion engineered waveguides in the presence of loss and identify a regime of pulse propagation dominated by

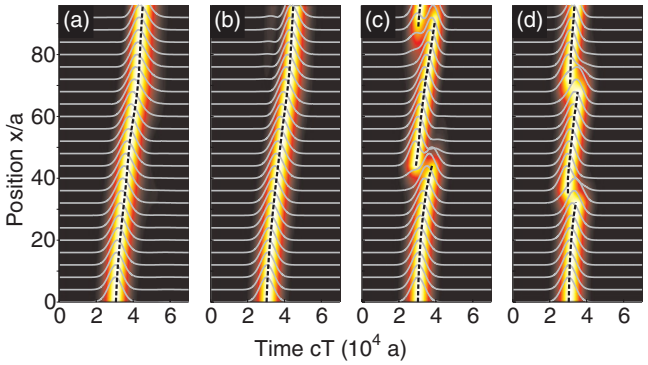

FIG. 6. (Color online) Numerical FDTD simulations of pulse propagation through a dispersion engineered slow-light waveguide for (a) $n_i = 0$, (b) $n_i = 2 \times 10^{-4}$, (c) $n_i = 1 \times 10^{-3}$, and (d) $n_i = 1.5 \times 10^{-3}$. Background coloring and gray curves show the normalized pulse profile as a function of time at different positions along the waveguide. Dashed black curve shows the trajectory of the pulse center of mass.

interference between the two hybrid states formed from the propagating and evanescent modes.

We consider the same PhC waveguide geometry as in Sec. IV, and launch spectrally narrow pulses with a full-width half-maximum of 0.02% of the central frequency, corresponding to a half width of $0.26456 \leqslant \omega a/2\pi c \leqslant 0.26461$ at $\omega_0 a/2\pi c = 0.264585$. To record the pulse dynamics in the slow-light section, field monitors were positioned every four lattice periods along the length of waveguide (ii) shown in Fig. 1(a).

We consider pulses launched at the inflection point frequency ω_0. Figure 6 illustrates the trajectory of pulses through the waveguide for three different values of loss. The horizontal axis corresponds to the normalized time, cT (units of a) and the vertical axis shows the position along the waveguide. At each position along the waveguide, the maximum pulse amplitude has been normalized to unity to allow an easy comparison of the pulse shape, even in the presence of strong loss. The dotted line passes through the pulse center of mass at each position. The local slope of this line, dx/dt, is approximately proportional to the local group velocity of the pulse.

Figure 6(a) shows the pulse dynamics for the lossless waveguide: The pulses maintain their shape as they propagate through the waveguide, with only a slight broadening due to dispersion. The change in slope at each end of the waveguide indicates the effect of the weakly decaying evanescent mode on the local group velocity of the pulse. Similar behavior is seen in Fig. 6(b) for $n_i = 2 \times 10^{-4}$, when the loss is still below the hybridization threshold shown in Fig. 3.

Figures 6(c) and 6(d), however, show strikingly different pulse behavior when the loss is increased above the threshold. The pulses change shape as they propagate, resulting in a periodic oscillation of the pulse trajectory, and a corresponding variation in the apparent group velocity from forward (positive) to backward (negative). This surprising behavior can be understood by considering the dispersion properties of the hybrid modes shown in Fig. 3. For $n_i > n_i^{\text{th}}$, there exist two modes at ω_0 with different $\text{Re}(k)$, but almost identical $\text{Im}(k)$. The incident pulse excites a superposition of the two modes which propagate along the waveguide, decaying at almost the same rate, but moving in and out of phase with each other due to the difference in $\text{Re}(k)$. The oscillation seen in Figs. 6(c) and 6(d) is a result of beating between these two modes, causing the pulse envelope to change shape such that at certain positions the peak intensity moves backward along the waveguide. The period of this oscillation can be predicted from the mode splitting in Fig. 3. For $n_i = 1 \times 10^{-3}$ ($n_i = 1.5 \times 10^{-3}$), $\Delta\text{Re}(k)a/2\pi = 0.0218(0.0276)$, corresponding to a beat length of $46a$ ($36a$). These values closely match the observed periods in Figs. 6(c) and 6(d). Note that the beating is not observed for $n_i < n_i^{\text{th}}$, since in this case the modes have equal $\text{Re}(k)$, so they remain in phase, while one of them decays much more rapidly with distance than the other.

VI. CONCLUSION

In conclusion, we have analyzed the influence of loss or gain on slow light associated with an inflection point of mode dispersion. We have developed a simple perturbation model that predicts the hybridization of propagating and evanescent waves and the associated reduction of effective loss or gain enhancement due to slow light. This effect is confirmed in numerical simulations, which also predict significant field enhancement even in the presence of strong losses. Remarkably, loss-induced mode hybridization strongly modifies pulse propagation dynamics, resulting in an oscillating pulse velocity between forward and backward directions in time. These results are generic to all waveguides that support inflection-point slow light and we anticipate their application in the study and design of slow-light waveguides based on photonic-crystal slabs, fibers, and plasmonic structures.

ACKNOWLEDGMENTS

This work was produced with the assistance of the Australian Research Council including the ARC Centers of Excellence program and Future Fellowship FT100100160. This work was supported by the NCI National Facility at the ANU.

[1] *Slow Light: Science and Applications*, edited by J. B. Khurgin and R. S. Tucker, (Tailor and Francis, New York, 2009).
[2] R. J. P. Engelen, Y. Sugimoto, Y. Watanabe, J. P. Korterik, N. Ikeda, N. F. van Hulst, K. Asakawa, and L. Kuipers, Opt. Express **14**, 1658 (2006).
[3] A. Y. Petrov and M. Eich, Appl. Phys. Lett. **85**, 4866 (2004).
[4] L. H. Frandsen, A. V. Lavrinenko, J. Fage-Pedersen, and P. I. Borel, Opt. Express **14**, 9444 (2006).
[5] T. Baba, Nature Photonics **2**, 465 (2008).
[6] J. Li, T. P. White, L. O'Faolain, A. Gomez-Iglesias, and T. F. Krauss, Opt. Express **16**, 6227 (2008).
[7] S. Kubo, D. Mori, and T. Baba, Opt. Lett. **32**, 2981 (2007).

[8] A. Karalis, J. D. Joannopoulos, and M. Soljačić, Phys. Rev. Lett. **103**, 043906 (2009).
[9] L. Dai, J. Xia, and C. Jiang, Appl. Opt. **50**, 4566 (2011).
[10] T. P. White, L. C. Botten, C. M. de Sterke, K. B. Dossou, and R. C. McPhedran, Opt. Lett. **33**, 2644 (2008).
[11] J. Ballato, A. Ballato, A. Figotin, and I. Vitebskiy, Phys. Rev. E **71**, 036612 (2005).
[12] A. Figotin and I. Vitebskiy, Waves Random Complex Media **16**, 293 (2006).
[13] E. Kuramochi, M. Notomi, S. Mitsugi, A. Shinya, T. Tanabe, and T. Watanabe, Appl. Phys. Lett. **88**, 041112 (2006).
[14] J. E. McMillan, X. D. Yang, N. C. Panoiu, R. M. Osgood, and C. W. Wong, Opt. Lett. **31**, 1235 (2006).
[15] R. W. Alexander, G. S. Kovener, and R. J. Bell, Phys. Rev. Lett. **32**, 154 (1974).
[16] K. C. Huang, E. Lidorikis, X. Y. Jiang, J. D. Joannopoulos, K. A. Nelson, P. Bienstman, and S. H. Fan, Phys. Rev. B **69**, 195111 (2004).
[17] A. R. Davoyan, W. Liu, A. E. Miroshnichenko, I. V. Shadrivov, Y. S. Kivshar, and S. I. Bozhevolnyi, Photonics Nanostruct.: Fundam. Appl. **9**, 207 (2011).
[18] N. Le Thomas, V. Zabelin, R. Houdré, M. V. Kotlyar, and T. F. Krauss, Phys. Rev. B **78**, 125301 (2008).
[19] J. Grgic, J. Pedersen, S. Xiao, and N. Mortensen, Photonics Nanostruct.: Fundam. Appl. **8**, 56 (2010).
[20] J. Grgić, S. Xiao, J. Mork, A.-P. Jauho, and N. A. Mortensen, Opt. Express **8**, 14270 (2010).
[21] W. T. Lu, Y. J. Huang, B. D. F. Casse, R. K. Banyal, and S. Sridhar, Appl. Phys. Lett. **96**, 211112 (2010).
[22] E. P. Fitrakis, T. Kamalakis, and T. Sphicopoulos, J. Opt. Soc. Am. B **28**, 2159 (2011).
[23] E. I. Kirby, J. M. Hamm, T. W. Pickering, K. L. Tsakmakidis, and O. Hess, Phys. Rev. B **84**, 041103 (2011).
[24] M. Tomita, T. Ueta, and P. Sultana, J. Opt. Soc. Am. B **28**, 1627 (2011).
[25] L. O'Faolain, S. A. Schulz, D. M. Beggs, T. P. White, M. Spasenović, L. Kuipers, F. Morichetti, A. Melloni, S. Mazoyer, J. P. Hugonin, P. Lalanne, and T. F. Krauss, Opt. Express **8**, 27627 (2010).
[26] M. Spasenović, T. P. White, S. Ha, A. A. Sukhorukov, T. Kampfrath, Y. S. Kivshar, C. M. de Sterke, T. F. Krauss, and L. Kuipers, Opt. Lett. **36**, 1170 (2011).
[27] S. Ha, M. Spasenović, A. A. Sukhorukov, T. P. White, C. M. de Sterke, L. K. Kuipers, T. F. Krauss, and Y. S. Kivshar, J. Opt. Soc. Am. B **28**, 955 (2011).
[28] H. G. Winful, Phys. Rep. **436**, 1 (2006).
[29] H. G. Winful, Phys. Rev. A **76**, 057803 (2007).
[30] J. P. Hugonin, P. Lalanne, T. P. White, and T. E. Krauss, Opt. Lett. **32**, 2638 (2007).
[31] S. Ha, A. A. Sukhorukov, K. B. Dossou, L. C. Botten, C. M. de Sterke, and Y. S. Kivshar, Opt. Lett. **34**, 3776 (2009).
[32] B. Corcoran, C. Monat, C. Grillet, D. J. Moss, B. J. Eggleton, T. P. White, L. O'Faolain, and T. F. Krauss, Nature Photonics **3**, 206 (2009).